Intranuclear Positions of HIV-1 Proviruses Are Dynamic and Do Not Correlate with Transcriptional Activity

Ryan C. Burdick,[a] Claire Deleage,[b] Alice Duchon,[c] Jacob D. Estes,[b,d] Wei-Shau Hu,[c] Vinay K. Pathak[a]

[a]Viral Mutation Section, HIV Dynamics and Replication Program, Center for Cancer Research, National Cancer Institute at Frederick, Frederick, Maryland, USA
[b]AIDS and Cancer Virus Program, Leidos Biomedical Research, Inc., Frederick National Laboratory for Cancer Research (FNLCR), Frederick, Maryland, USA
[c]Vaccine and Gene Therapy Institute and Oregon National Primate Research Center, Oregon Health & Science University, Beaverton, Oregon, USA
[d]Viral Recombination Section, HIV Dynamics and Replication Program, Center for Cancer Research, National Cancer Institute at Frederick, Frederick, Maryland, USA

ABSTRACT The relationship between spatiotemporal distribution of HIV-1 proviruses and their transcriptional activity is not well understood. To elucidate the intranuclear positions of transcriptionally active HIV-1 proviruses, we utilized an RNA fluorescence *in situ* hybridization assay and RNA stem loops that bind to fluorescently labeled bacterial protein (Bgl-mCherry) to specifically detect HIV-1 transcription sites. Initially, transcriptionally active wild-type proviruses were located closer to the nuclear envelope (NE) than expected by random chance in HeLa (~1.4 μm) and CEM-SS T cells (~0.9 μm). Disrupting interactions between HIV-1 capsid and host cleavage and polyadenylation specificity factor (CPSF6) resulted in localization of proviruses to lamina-associated domains (LADs) adjacent to the NE in HeLa cells (~0.9 - 1.0 μm); however, in CEM-SS T cells, there was little or no shift toward the NE (~0.9 μm), indicating cell-type differences in the locations of transcriptionally active proviruses. The distance from the NE was not correlated with transcriptional activity, and transcriptionally active proviruses were randomly distributed throughout the HeLa cell after several cell divisions, indicating that the intranuclear locations of the chromosomal sites of integration are dynamic. After nuclear import HIV-1 cores colocalized with nuclear speckles, nuclear domains enriched in pre-mRNA splicing factors, but transcriptionally active proviruses detected 20 h after infection were mostly located outside but near nuclear speckles, suggesting a dynamic relationship between the speckles and integration sites. Overall, these studies establish that the nuclear distribution of HIV-1 proviruses is dynamic and the distance between HIV-1 proviruses and the NE does not correlate with transcriptional activity.

IMPORTANCE HIV-1 integrates its genomic DNA into the chromosomes of the infected cell, but how it selects the site of integration and the impact of their location in the 3-dimensional nuclear space is not well understood. Here, we examined the nuclear locations of proviruses 1 and 5 days after infection and found that integration sites are first located near the nuclear envelope but become randomly distributed throughout the nucleus after a few cell divisions, indicating that the locations of the chromosomal sites of integration that harbor transcriptionally active proviruses are dynamic. We also found that the distance from the nuclear envelope to the integration site is cell-type dependent and does not correlate with proviral transcription activity. Finally, we observed that HIV-1 cores were localized to nuclear speckles shortly after nuclear import, but transcriptionally active proviruses were located adjacent to nuclear speckles. Overall, these studies provide insights into HIV-1 integration site selection and their effect on transcription activities.

KEYWORDS HIV-1, capsid, CPSF6, integration, transcription

Reverse transcription of the HIV-1 single-stranded RNA genome into double-stranded DNA (vDNA), release of the vDNA from the capsid in the cell nucleus, and integration of the vDNA into the host cell genome are critical steps in HIV-1 replication (1). Lens

epithelium-derived growth factor (LEDGF)/p75, a protein that binds to nucleosomes of transcriptionally active genes, binds to HIV-1 integrase and directs integration into transcriptionally active and highly spliced genes (2–4). The HIV-1 integrase-LEDGF/p75 interaction facilitates HIV-1 replication because integration into transcriptionally active genes directly influences the level of HIV-1 gene expression and virus production. The HIV-1 capsid binds to cleavage and polyadenylation specificity factor 6 (CPSF6), a host protein that is one subunit of a cleavage factor required for 3′ RNA cleavage and polyadenylation, which promotes integration into euchromatin (5–9). Although the mechanism by which CPSF6 influences integration targeting is not known, CPSF6 mediates the nuclear import of intact viral cores (1, 10), and potentially facilitates the transport of the viral cores to the site of integration prior to uncoating (6, 9).

Lamina-associated domains (LADs) are heterochromatin-rich regions near the nuclear lamina and are typically associated with transcription repressive chromatin and low gene expression (11). It is presumed that HIV-1, like other lentiviruses, must avoid the repressive heterochromatin areas located near the nuclear envelope (NE) immediately following nuclear import, and transport to the transcriptionally active chromatin regions. Recent evidence indicates that HIV-1 integrates into nuclear speckle-associated genomic domains (12). Nuclear speckles are membrane-free subcompartments that are enriched in splicing factors, transcription factors, and chromatin remodeling factors (reviewed in reference [13]). Nuclear speckles are located in interchromatin nuclear space and contain few, if any, genes but are often formed near highly active transcription sites (reviewed in reference [14]). It was recently reported that unintegrated vDNA localizes to nuclear speckles (15), but the location of integrated vDNAs was not determined. An understanding of the nuclear positioning of HIV-1 integration, and the viral and host factors involved in integration site selection is critical for elucidating this fundamental aspect of HIV-1 replication.

Previous studies have sought to determine the nuclear location of HIV-1 reverse transcription complexes/preintegration complexes (RTCs/PICs) and HIV-1 integration. We and others used various fluorescent protein-tagged viral proteins, including integrase and capsid, or fluorescent protein-tagged host restriction factors that specifically incorporate into virions, including APOBEC3F (A3F) and APOBEC3G, to track HIV-1 into the nuclei of infected cells (1, 16–23). Other studies have visualized HIV-1 nucleic acid using various approaches, including fluorescence *in situ* hybridization assays (6, 9, 24, 25), incorporation of a fluorescently labeled thymidine analog, 5-ethynyl-2′-deoxyuridine (EdU) into nascent vDNA using click chemistry (26–28), and immunofluorescence detection of repair foci for double-strand DNA breaks specifically induced in the HIV-1 provirus by heterologous expression of the I-SceI endonuclease (23, 29). We previously estimated that only 1 of ~50 RTCs/PICs in infected cells results in provirus formation and productive infection (17), indicating a low particle-to-infectivity ratio. However, most previous studies have not specifically determined the nuclear location of the RTCs/PICs that lead to productive infection, and the nuclear positioning of noninfectious RTCs/PICs may not reflect the nuclear positioning of infectious RTCs/PICs. Additionally, many studies that visualized HIV-1 DNA (vDNA) did not discriminate between integrated vDNA and unintegrated vDNA. Unintegrated vDNA is not likely to significantly contribute to HIV-1 replication (reviewed in reference 30) because of low transcriptional activity due to NP220-mediated repression (31, 32).

Here, we developed and validated a next-generation fluorescence *in situ* hybridization approach to detect HIV-1 RNA (33) and used a previously described RNA stem-loop technology (21, 34) to specifically detect transcriptionally active proviruses (here referred to as "active proviruses") and provide further evidence that HIV-1 preferentially integrates into genes located near (~1.4 μm) the nuclear periphery. We find that the nuclear positioning of active proviruses is influenced by the CA-CPSF6 interaction, but the degree to which CA-CPSF6 influences this nuclear positioning is cell-type dependent. We also observe that the integrase-LEDGF/p75 interaction was less important for nuclear positioning of active proviruses but was more critical for HIV-1 transcription than CPSF6. Finally, we demonstrate the utility of manipulating HIV-1 integration into different chromatin regions to provide new
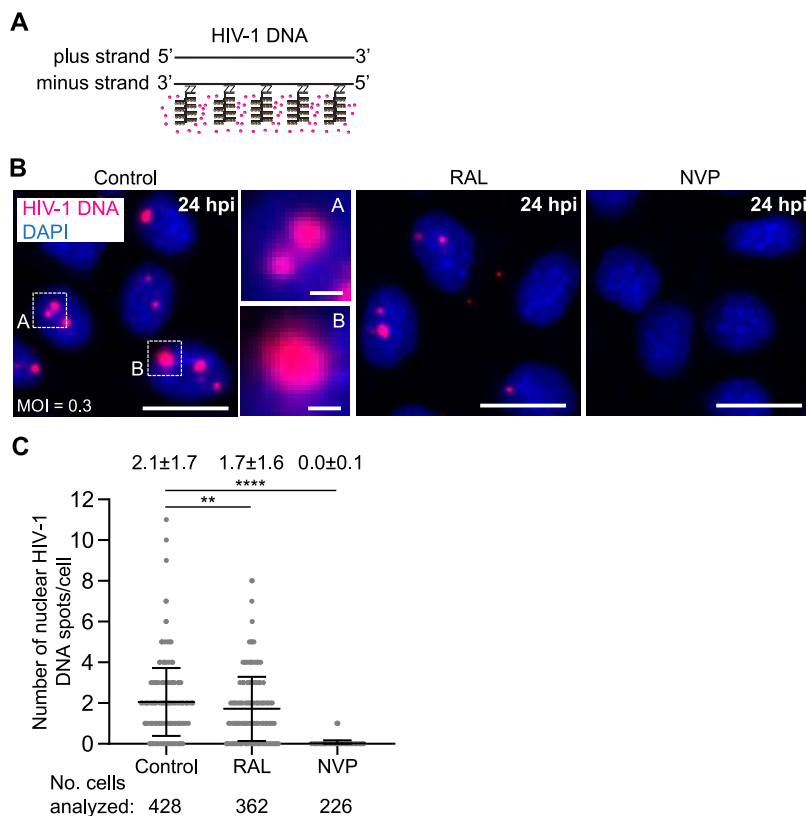
FIG 1 Detection of integrated and unintegrated HIV-1 DNA 24 hpi using DNAscope. (A) Schematic of an HIV-1 specific DNAscope *in situ* hybridization assay. 78 pairs of Z probes target the minus-strand HIV-1 DNA. After a cascade of hybridization events, probes labeled HRP (brown circles) bind the amplifier probes and catalyze the deposition of Cy3.5 fluorophores (red circles) for single-copy detection of HIV-1 DNA. (B) HeLa cells were infected with an amount of virus that leads to ~30% of cells expressing GFP reporter 48 hpi (MOI = 0.3) in the presence of a DMSO control (left), integrase inhibitor raltegravir (RAL; middle), and reverse transcriptase inhibitor nevirapine (NVP; right) and fixed at 24 hpi. HIV-1 DNA (red) was detected by DNAscope and cell nuclei were counterstained using DAPI (blue). Scale bar, 10 μm; inset scale bar, 1 μm. (C) The number of nuclear HIV-1 DNA spots were determined for cells treated with the DMSO control, RAL, or NVP. Each dot represents a nucleus; lines indicate mean; statistical significance was determined using Mann-Whitney U tests. ****, $P < 0.0001$; **, $P < 0.01$.

insights into the three-dimensional organization of the human genome and transcription activity.

RESULTS

Development of a method to detect HIV-1 DNA. To detect vDNA, HeLa cells treated with the DMSO control, integrase inhibitor raltegravir (RAL), or reverse transcriptase inhibitor (NVP) were infected with a single-cycle HIV-1 GFP reporter virus at a multiplicity of infection (MOI) of 0.3 (~30% *gfp* positive cells 48 h after infection). At 24 h postinfection (hpi), vDNA was detected using an HIV-specific DNAscope *in situ* hybridization assay (33). Briefly, the branched DNA *in situ* hybridization technique utilizes 78 pairs of Z probes that specifically target HIV-1 minus-strand DNA (Fig. 1A and B). The Z probe pairs anneal to adjacent target sequences, ensuring amplification of target-specific signals. After a cascade of hybridization events, in which the penultimate step is the hybridization of horseradish peroxidase (HRP)-labeled probes to the amplifier probes, the covalent deposition of Cy3.5 fluorophore adjacent to the probes is catalyzed by HRP allowing single-molecule detection of vDNA. An average of 2.1 vDNA foci/nucleus was detected in the control cells (Fig. 1C; range from 0 to 11), indicating that only 1 in ~7 nuclear vDNAs leads to GFP reporter expression. The average number of vDNA foci/nucleus was only slightly lower for RAL-treated cells compared to control cells (1.7 versus 2.1, respectively; range from 0–8), indicating unintegrated vDNA can be efficiently detected 24 hpi. As expected, very few NVP-treated cells (1 of 226) contained a

single vDNA focus. The large size of the vDNA foci (Fig. 1B) resulting from the large amount of Cy3.5 fluorophore deposited adjacent to the vDNA, and the inability to discriminate between integrated and unintegrated vDNA, precluded the determination of intranuclear locations of integrated proviruses. Nevertheless, these results showed that DNAscope can be used to efficiently detect vDNA in infected cells with single-molecule sensitivity.

Development of a method to specifically detect active proviruses. HIV-1 RNA (vRNA) was detected at the single-molecule level using the RNAscope *in situ* hybridization assay with a series of 78 pairs of Z probes that specifically target plus-strand vRNA (Fig. 2A, top). HeLa cells were infected with single-cycle HIV-1 GFP reporter virus at an MOI of 0.05 and vRNA was detected 24 hpi. Infected cells expressing various levels of vRNA could be observed 24 hpi (Fig. 2A, bottom). Although vRNA was detected using probes labeled with Alexa Fluor 488, a fluorescent dye which has a similar emission spectrum as GFP, the expression of the GFP reporter did not interfere with vRNA detection because the GFP protein was damaged with formalin fixation, precluding its detection. The percentage of cells expressing vRNA at 24 hpi (~4.0%; Fig. 2B) was similar to the percentage of cells that expressed the GFP reporter 48 hpi (~3.7%; Fig. 2C). Treatment of the cells with NVP or RAL significantly decreased the proportion of cells expressing vRNA (Fig. 2B) and GFP reporter (Fig. 2C), indicating that both reverse transcription and integration was required for detection of vRNA when the cells were infected at a low MOI. Upon close inspection, a single, bright focus containing multiple RNAs could be readily detected in most cells expressing vRNA (Fig. 2D and E). To determine if the bright foci were HIV-1 transcription sites (TS) and not sites of vRNA aggregation, vRNA and vDNA was simultaneously detected in a HeLa clone containing two proviruses (Fig. 2F). The average number of observed vDNA foci/nucleus (1.8) was similar to the expected number of vDNA foci/nucleus (2.0), indicating a high efficiency of DNA detection (90%; Fig. 2G). The percentage of putative HIV-1 TSs that colocalized with vDNA was high (83%; Fig. 2H) and similar to the vDNA detection efficiency (90%), indicating that most, if not all, of the bright nuclear foci are HIV-1 TSs.

Intranuclear localization of active proviruses at 24 hpi and 5 dpi. To determine the nuclear positions of active proviruses, we measured the distance between each HIV-1 TS and the nuclear boundary in HeLa cells 24 hpi using a custom MATLAB program. The radial distances between the HIV-1 TSs and the NE, defined by the sharp decrease in DAPI signal, were significantly smaller than the radial distances between random positions (see Materials and Methods for determination of random positions) in the nucleus and the NE (~1.4 μm versus ~1.7 μm, respectively; $P < 0.0001$; Fig. 2I). These results indicate the active proviruses are located closer to the nuclear periphery than would be expected if they were randomly distributed in the nucleus. These distances were similar to our previous measurements of the distance between A3F-YFP- and integrase-YFP-labeled HIV-1 RTCs/PICs and the NE shortly after nuclear import (~1.4 μm) (21), indicating viruses are at or near the target site of integration shortly after nuclear import. Next, we measured the distance between HIV-1 TSs and the NE at 5 dpi after multiple rounds of cell division (Fig. S1). The distances between the HIV-1 TSs and the NE at 5 dpi were significantly larger than the distances measured at 24 hpi (~1.8 μm; $P < 0.0001$; Fig. 2I). These results are consistent with a previous report indicating proviruses were randomly distributed 13 dpi, (23). In this previous study, the randomly distributed proviruses were detected whether or not they were transcriptionally active. The distances between HIV-1 TSs and the NE at 5 dpi in cells treated with aphidicolin (APC), an inhibitor of nuclear DNA replication that blocks cell division, were similar to the distances measured at 24 hpi. These results provide direct evidence that cell division is required for the change in locations of active proviruses away from the NE. We also determined the distances between the host gene glyceraldehyde 3-phosphate dehydrogenase (GAPDH) TSs and the NE and found that these distances were similar to the distances of HIV-1 TS and NE 5 dpi (Fig. 2I). Taken together, these results indicate that the intranuclear positions of chromatin regions that are targets for integration and harbor active proviruses can be dynamic and change after cell division.

LEDGF/p75 is a ubiquitous nuclear protein that binds to HIV-1 integrase and facilitates HIV-1 replication by directing integration into genes that are transcriptionally active and highly spliced (2–4). We visualized HIV-1 TSs 24 hpi in a previously described HeLa cell line
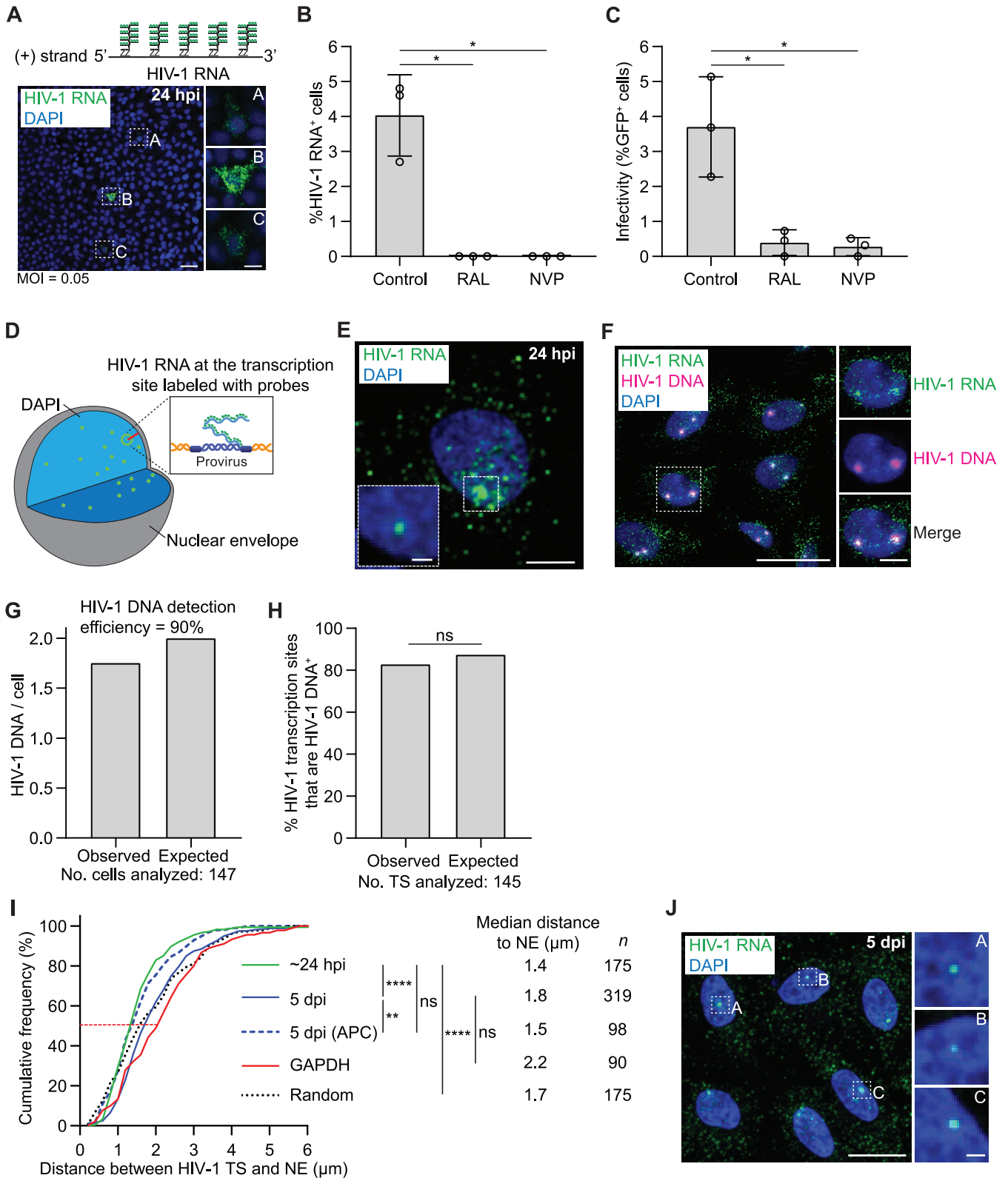
FIG 2 Detection of HIV-1 RNA and HIV-1 transcription sites (TSs) using RNAscope. (A) HeLa cells were infected with an amount of virus that leads to ~5% of cells expressing GFP reporter 48 hpi (MOI = 0.05) and fixed 24 hpi. HIV-1 RNA was detected by RNAscope, an RNA *in situ* hybridization assay which uses probes labeled with Alexa Fluor 488 (green); cell nuclei were counterstained using DAPI (blue). Scale bar, 40 μm; inset scale bar, 10 μm. (B and C) The percentage of HIV-1 RNA^{+} cells ~24 hpi (B) and percentage of GFP^{+} cells ~48 hpi (C) was determined for cells treated with the DMSO control, RAL, or NVP. Data are mean ± SD; statistical significance was determined using Welch's t-tests. (D) Schematic showing HIV-1 RNA at the TS labeled with FISH probes in a nucleus counterstained with DAPI. Red line indicates the closest distance in 3 dimensions between the center of the HIV-1 TS and the edge of

in which LEDGF/p75 was deleted using CRISPR/cas9 (HeLa:LKO [21]). We observed some infected cells that expressed HIV-1 RNA and had a detectable TS, while other cells expressed HIV-1 RNA but did not have a detectable TS (Fig. 3A). A lower percentage of infected HeLa:LKO cells (i.e., HIV-1 RNA expressing) had detectable TSs compared to infected control HeLa cells (29% versus 64%, respectively; Fig. 3B). Since the detection of TSs requires active transcription at the time of fixation, proviruses in vRNA+ cells that are transcriptionally silent at the time of fixation due to stochastic nature of transcription (35, 36) will not be detected. These observations suggest that proviruses in the HeLa:LKO cells are more likely to be transcriptionally silent at the time of fixation. The nuclear locations of proviruses that were never transcriptionally active (vRNA-) could not be detected in this assay.

The median distance between the HIV-1 TSs and the NE in HeLa and HeLa:LKO cells was similar ($\sim$1.4 μm; $P > 0.05$; Fig. 3C), indicating that chromatin regions that are targets for integration in the presence or absence of LEDGF/p75 and harbor active proviruses are located a similar distance from the nuclear periphery. The fluorescence intensity of HIV-1 TSs, which is expected to directly correlate with the number of nascent vRNAs at the TS, was significantly lower in HeLa:LKO cells compared to HeLa cells, as expected from our previous studies (Fig. 3D; [21]). These results indicate that the fluorescence intensity of the TS can be used as a semiquantitative measurement of proviral transcription activity.

Some studies have suggested a functional link between the radial position of a gene and its activity; those that are located toward the interior of the nucleus tend to be more transcriptionally active compared to genes closer to the NE (reviewed in reference 37). However, it has also been demonstrated that alteration of the radial position of genes does not affect expression, and that many genes do not undergo positional changes when their expression levels are modulated (reviewed in reference 37). Therefore, we performed a linear regression analysis to determine the relationship between the HIV-1 TS fluorescence intensity and the distance between the HIV-1 TS and the NE (Fig. 3E). The results indicated that there was no correlation between the HIV-1 TS fluorescence intensity and their distance to the NE at 24 hpi ($r = 0.08$, $P > 0.05$), 5 dpi ($r = 0.05$, $P > 0.05$), 24 hpi in HeLa:LKO cells ($r = 0.04$, $P > 0.05$), or 5 dpi in APC-treated cells ($r = -0.13$, $P > 0.05$). There was also no correlation between GAPDH TS fluorescence and their distance to the NE ($r = 0.01$, $P > 0.05$). Consistent with previous observations (38), there was wide variation in the distances from the GAPDH TSs and the NE (0.5 μm to 5.8 μm; Fig. 3E), indicating that the intranuclear locations of at least some genes are not fixed and can be altered after cell division. Thus, the radial distance between HIV-1 proviruses or the GAPDH gene and the NE is not correlated with transcription activity.

The CA-CSPF6 interaction influences the intranuclear location of integration. CPSF6 is a nuclear host factor that binds to the HIV-1 capsid (39) and disruption of CA-CPSF6 interactions alters the target sites of HIV-1 integration (5–8). Similar to HIV-1 encoding WT CA, HIV-1 TSs could also be detected 24 h after infection for the CPSF6-binding capsid mutants N74D (5) and A77V (40), as previously described (1) (Fig. 4A). The fluorescence intensities of the HIV-1 TSs for the N74D and A77V mutants were similar to the WT, indicating that, unlike integration in the absence of LEDGF/p75, integration with impaired CA-CPSF6 interaction does not affect HIV-1 transcription levels (Fig. 4B). These results are consistent with previous observations that CA-CPSF6 binding mutants (N74D or A77V) have similar infectivities as WT (1, 40). To elucidate the role of CPSF6 in nuclear positioning of active proviruses, we first determined the distance between the HIV-1 TS and the NE for N74D and A77V capsid mutants

FIG 2 Legend (Continued)
the DAPI signal (NE). (E) Detection of HIV-1 TS 24 hpi. Scale bar, 10 μm; inset scale bar, 2 μm. The contrast of the inset was adjusted to show the HIV-1 TS. (F) Simultaneous detection of HIV-1 RNA and DNA. HIV-1 RNA and DNA were simultaneously detected in a clonal population of cells derived from a single infected cell containing two HIV-1 proviruses. The images show that HIV-1 TSs colocalize with HIV-1 DNA. Scale bar, 40 μm; inset scale bar, 10 μm. (G) The DNA detection efficiency (90%) was calculated by dividing the observed number of HIV-1 DNA nuclear spots/cell (1.8) by the expected number of HIV-1 DNA nuclear spots/cell (2.0). (H) The percentage of putative HIV-1 TSs that colocalized with HIV-1 DNA. P value is from Fisher's exact test; ns, not significant ($P > 0.05$). (I) Cumulative frequency distribution of distances (μm) between HIV-1 TS detected 24 hpi and NE, HIV-1 TS detected 5 dpi and NE, HIV-1 TS detected in aphidicolin (APC)-treated cells 5 dpi and NE, GAPDH TS and NE, and random intranuclear positions and NE; median distances are indicated by red dotted line. Statistical significance was determined using Kolmogorov-Smirnov tests. The sample number (n) indicates number of TSs analyzed. (J) Detection of HIV-1 RNA and HIV-1 TSs by FISH 5 dpi. Scale bar, 20 μm; inset scale bar, 2 μm. The contrast of the inset was adjusted to show the HIV-1 TS. ****, $P < 0.0001$; **, $P < 0.01$; *, $P < 0.05$.
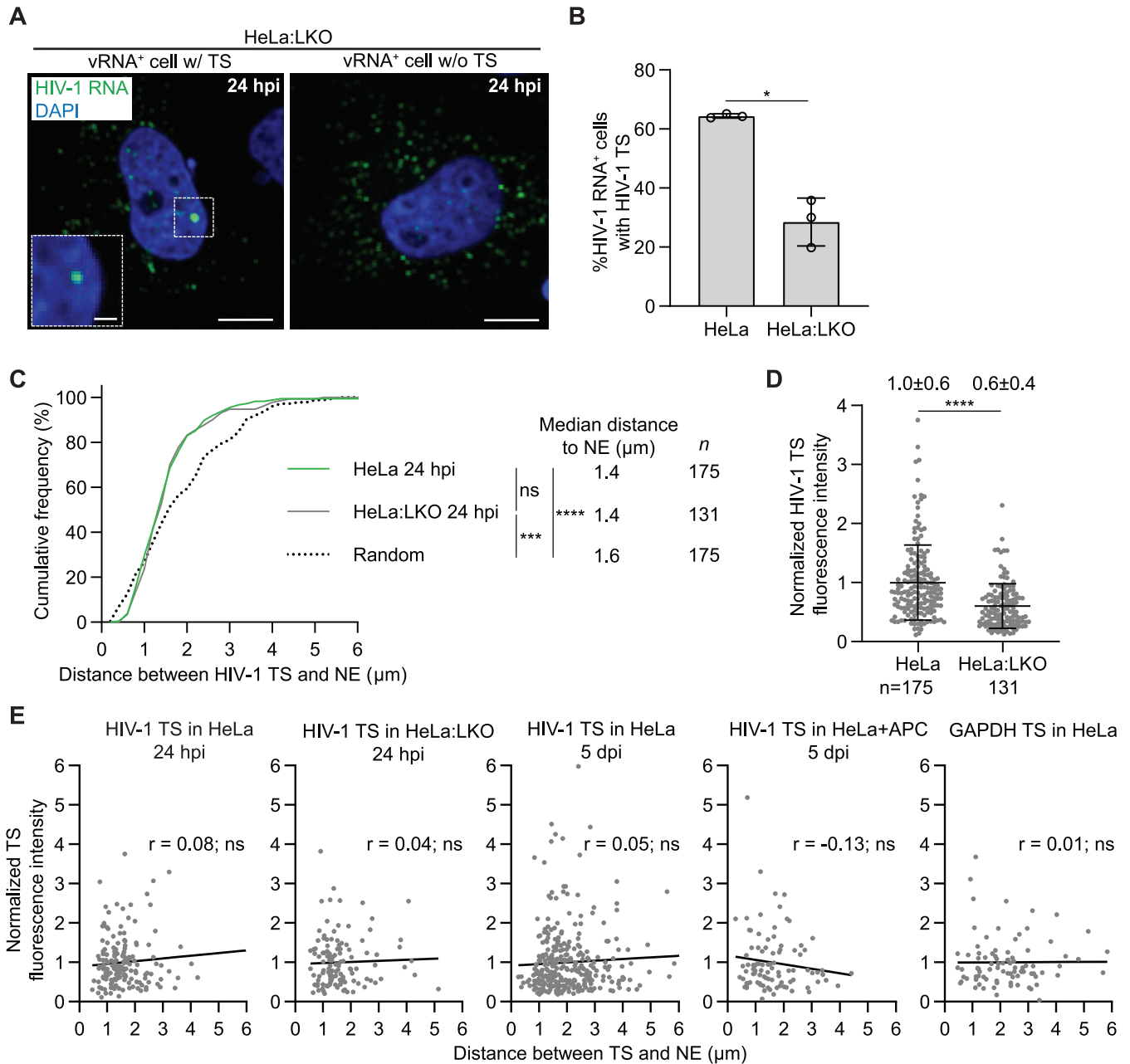
FIG 3 Detection of HIV-1 TSs in LEDGF knockout cells and determination of HIV-1 TS fluorescence intensities. (A) HeLa:LEDGF/p75 knockout (LKO) cells were infected and fixed 24 hpi. HIV-1 RNA was detected by FISH probes labeled with Alexa Fluor 488 (green) and cell nuclei were counterstained using DAPI (blue). Scale bar, 10 μm. (B) The percentage of infected cells with detectable HIV-1 TSs. Parental HeLa cells or HeLa-LEDGF knockout (LKO) cells were infected with an amount of virus that leads to ~5% of cells expressing GFP reporter 48 hpi (MOI = 0.05) and fixed 24 hpi. HIV-1 TSs were detected by RNA FISH and cell nuclei were counterstained using DAPI. Statistical significance was determined using a Welch's t test. (C) Cumulative frequency distribution of distances (μm) between HIV-1 TS and NE in HeLa and HeLa:LKO cells detected 24 hpi and between random intranuclear positions and NE. Statistical significance was determined using Kolmogorov-Smirnov tests. The sample number (n) indicates number of HIV-1 TSs analyzed. The HIV-1 TSs for HeLa cells 24 hpi and random positions are replotted from Fig. 2I (D) The normalized fluorescence intensity of the HIV-1 TSs in HeLa and HeLa:LKO cells. Lines are mean $\pm$ SD; P values are from Welch's t-tests. (E) Linear regression analysis of TS fluorescence intensity and distance between TSs and NE for HIV-1 TSs in HeLa cells ~24 hpi, HeLa:LKO cells 24 hpi, HeLa cells 5 dpi, and APC-treated HeLa cells 5 dpi and GAPDH TSs in HeLa cells. The Pearson correlation coefficient (r) was determined. ****, $P < 0.0001$; ***, $P < 0.001$; *, $P < 0.05$; ns, not significant ($P > 0.05$).

detected at 24 hpi (Fig. 4C). The TSs for the N74D and A77V CA mutants were located much closer (~0.9 -1.0 μm) to the nuclear periphery compared to WT virus (~1.3 μm), indicating that impairment of CA-CPSF6 interactions results in HIV-1 integration into chromatin regions that are closer to the NE (Fig. 4C). We also determined whether the nuclear location of the active proviruses for the N74D and A77V CA mutants changed after cell division. The distance between the HIV-1 TS and the NE for the N74D and A77V CA mutants was shifted toward the
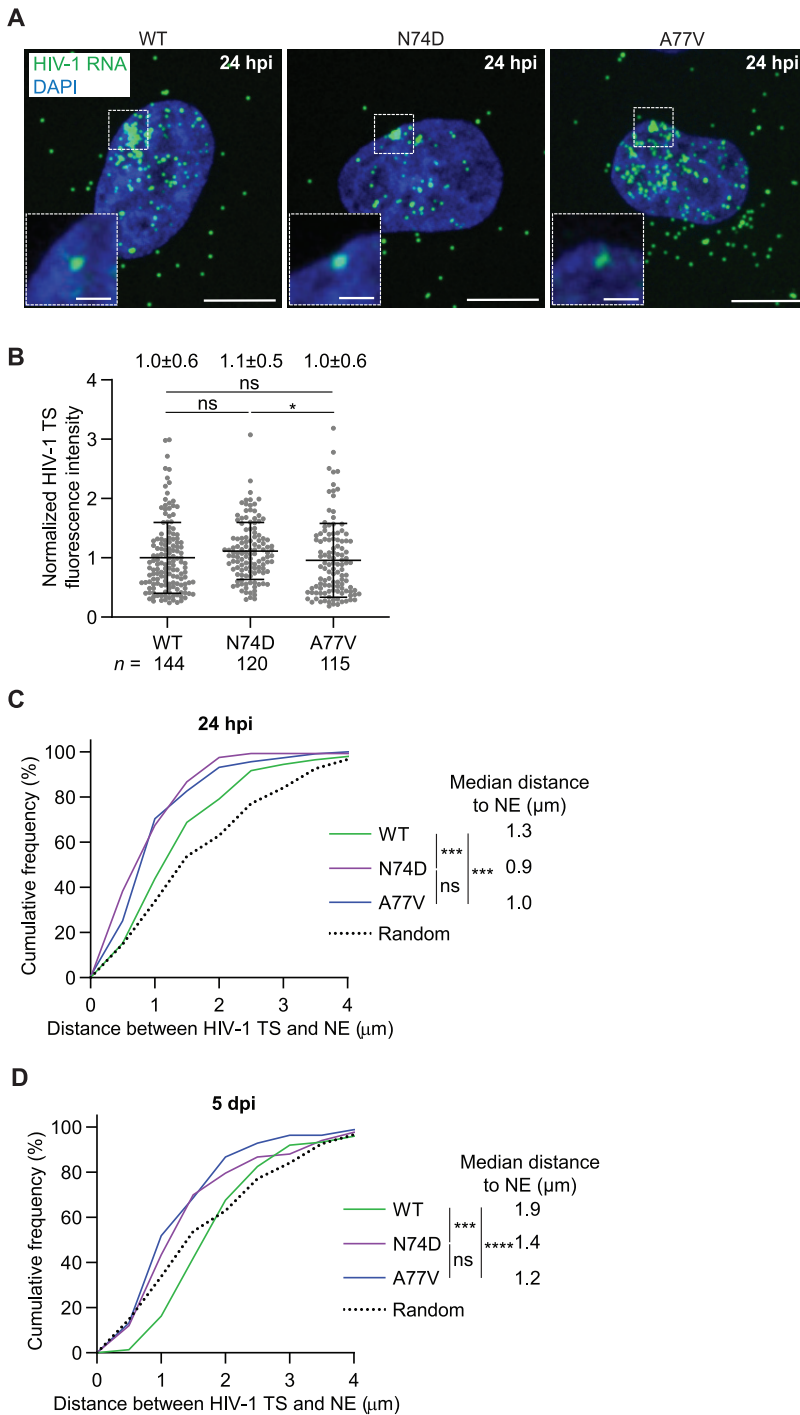
FIG 4 Effect of CA-CPSF6 binding on the intranuclear positions of active proviruses. (A) Detection of HIV-1 RNA and HIV-1 TSs by RNAscope using probes labeled with Alexa Fluor 488 (green) 24 hpi of HeLa cells with HIV-1 containing capsid mutations N74D or A77V. The nuclei were stained with DAPI (blue). Scale bar, 10 μm; inset scale bar, 2 μm. The contrast of the insets was adjusted to show the HIV-1 TS. (B) Normalized fluorescence intensity of the HIV-1 TSs derived from WT, N74D, or A77V virus in HeLa cells. Lines are mean $\pm$ SD; Statistical significance was determined using Welch's t-tests. (C and D) Cumulative frequency distribution of distances (μm) between HIV-1 TS and NE for WT, N74D, and A77V virus in HeLa cells detected 24 hpi (C) and 5 dpi (D). Statistical significance was determined using Kolmogorov-Smirnov tests. ****, $P < 0.0001$; ***, $P < 0.001$; *, $P < 0.05$; ns, not significant ($P > 0.05$).

interior of the nucleus at 5 dpi (1.2–1.4 μm at 5 dpi versus 0.9–1.0 μm at 24 hpi), although the positions of the proviruses were still significantly more peripheral than WT HIV-1 TSs (Fig. 4D). These results are consistent with a report indicating that lamina-associated domains (LADs) interact either with the NE or the outer surface of nucleoli, and that ~30% of the chromosomal regions defined as LADs are at the nuclear periphery during interphase (41). In summary, the active proviruses derived from virus harboring CA mutants with impaired binding to CPSF6 have similar levels of transcriptional activity but are more likely to be located closer to the NE than WT proviruses.

Intranuclear positioning of active proviruses in T cells. Next, we sought to determine the intranuclear positioning of active proviruses in T lymphocytes, the natural target of HIV-1 infection. However, detecting RNA in nonadherent T cells using the RNAscope assay without perturbing their normal cell morphology is challenging. Therefore, we utilized a previously described RNA stem-loop technology (21, 34) to specifically detect vRNA. The HIV-1 genome was engineered with 18 copies of a stem-loop structure (BglSL) in place of the *vif* and *vpr* genes (Fig. 5A, top). Infection of cells expressing a fluorescently labeled bacterial BglG protein (Bgl-mCherry) results in the specific labeling of vRNA containing BglSL and detection of HIV-1 TSs under certain imaging conditions (Fig. 5A, bottom). Typically, low laser power imaging conditions are used to facilitate the observation of the HIV-1 TS, which contains multiple copies of vRNA. Under these conditions, the vRNAs that move away from the TS have signals that are below the limit of detection. To determine if the detection of HIV-1 TSs by RNAscope or the BglSL assays yield similar results, we compared the distances between HIV-1 TSs and the NE in HeLa cells 24 hpi (Fig. 5B). The distribution of distances between the HIV-1 TSs and the NE determined using each technique was similar (median distances of ~1.3 and ~1.4 μm, respectively; $P > 0.05$). These results indicate that both techniques provide almost identical measurements of the distance between active proviruses and the NE.

Next, we generated a CEM-SS T cell line that stably expresses Bgl-mCherry (CEM-SS: Bgl-mCherry). CEM-SS T cells are frequently used for HIV-1 infection and replication studies (42–45). These cells were infected with HIV-1 containing BglSL (and a *gfp* reporter gene in place of *nef*) and the HIV-1 TSs were visualized by live-cell imaging 24 hpi (Fig. 1C). The HIV-1 TSs derived from virus containing WT CA were located near the nuclear periphery (~0.9 μm) and were significantly more peripheral than would be expected if they were randomly distributed in the nucleus (~1.6 μm; Fig. 5D). Interestingly, the distances between the active proviruses and the NE in HeLa cells are larger than the distances measured in CEM-SS cells (~1.3 versus ~0.9 μm), but this could be explained in part by the larger nucleus size of HeLa cells compared to CEM-SS cells (average radius of 7.6 μm and 6.4 μm, respectively; Fig. 5E). The average distance between the active proviruses and the NE in HeLa cells represents ~17% of the distance to the center of the nucleus (1.3 μm/7.6 μm = 0.17). Similarly, the average distance between the active proviruses and the NE in CEM-SS cells is ~14% of the distance to the center of the nucleus (0.9 μm/6.4 μm = 0.14). However, the normalized distances between the HIV-1 TS and the NE in HeLa and CEM-SS cells were significantly different ($P = 0.0255$), suggesting that factors other than nuclear size, such as differences in chromatin organization, may contribute to differences in intranuclear positioning of actives proviruses.

We also determined the distance between each HIV-1 TS and the NE for the N74D and A77V CA mutant viruses; unlike the results in HeLa cells, these distances were similar (~0.9 μm) to the locations of HIV-1 TSs derived from WT virus (Fig. 5D). These observations indicated that the chromosomal regions that are targets of integration and harbor active proviruses for the N74D, A77V, and WT viruses are located a similar distance from the NE. We previously observed that WT viral cores, but not N74D and A77V viral cores, enter the nucleus of CEM-SS T cells (1); these results indicate that although the uncoating location of WT and N74D/A77V viral cores may differ in CEM-SS cells, the vDNA integrates into chromatin located close to the nuclear periphery.

Active proviruses do not colocalize with nuclear speckles. We sought to determine the role of nuclear speckles at two different time points during the early stage of HIV-1 infection. Nuclear speckles were identified by indirect immunostaining of the nuclear splicing factor SC35 (Fig. 6A), a protein that is highly enriched in nuclear speckles (reviewed in reference 13). To determine whether HIV-1 cores localize to nuclear speckles
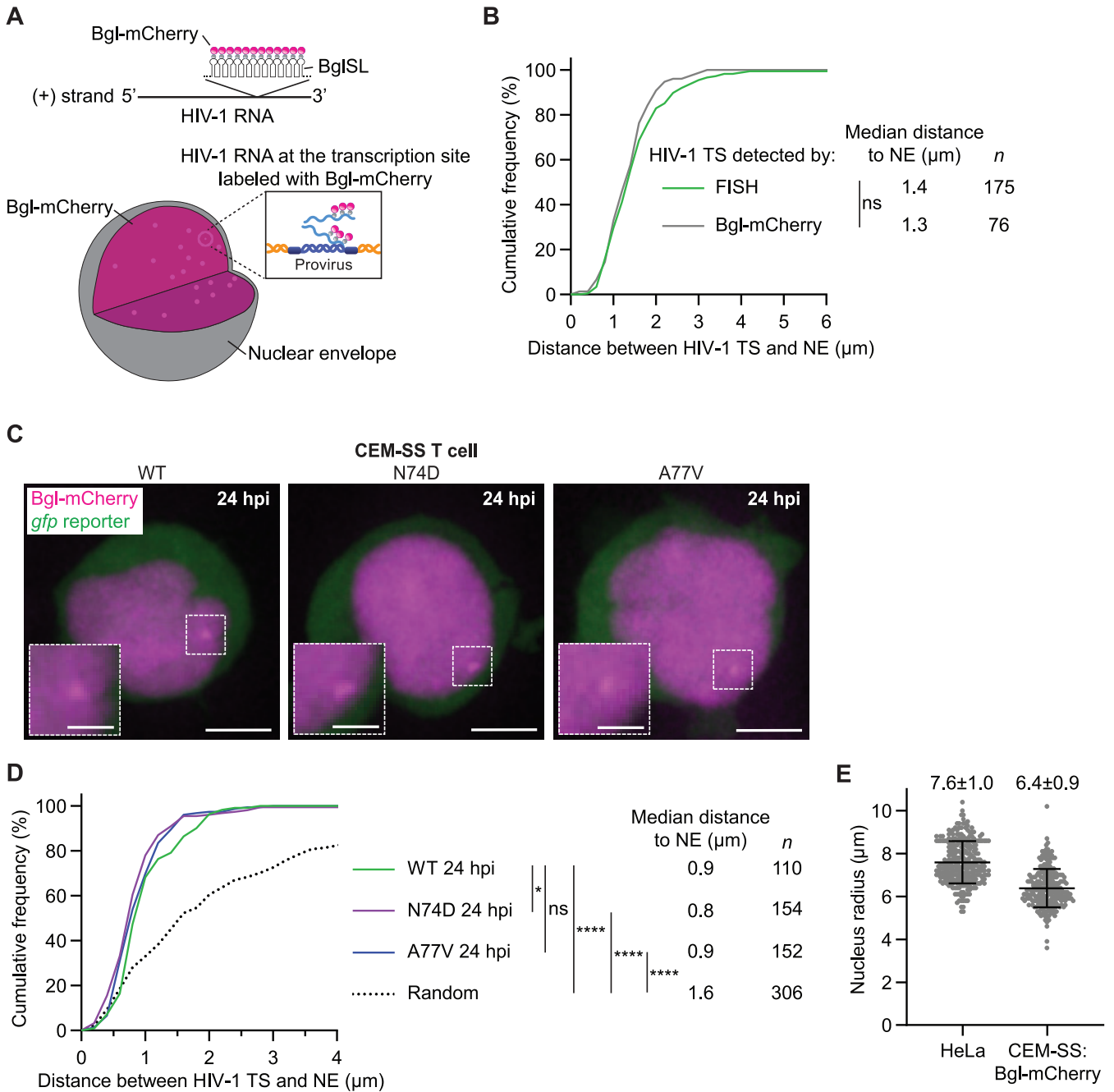
FIG 5 Detection of HIV-1 TSs in CEM-SS T cells. (A) Schematic showing HIV-1 RNA containing Bgl-G stem-loops (BglSL) that are bound to Bgl-mCherry (top) and HIV-1 RNA at the TS labeled with Bgl-mCherry (bottom). Bgl-mCherry protein that is not bound to HIV-1 RNA is diffusely distributed in the nucleus and can be used to define the nuclear boundary. (B) Cumulative frequency distribution of distances (μm) between HIV-1 TSs and NE for HIV-1 RNA in HeLa cells detected by RNAscope detected 24 hpi or for HIV-1 RNA containing BglSL in HeLa cells expressing Bgl-mCherry 24 hpi. (C) CEM-SS T cells expressing Bgl-mCherry were infected with WT, N74D, or A77V virus containing BglSL and HIV-1 TSs were detected 24 hpi. Scale bar, 10 μm; inset scale bar, 2 μm. (D) Cumulative frequency distribution of distances (μm) between HIV-1 TSs detected 24 hpi and NE for WT, N74D, and A77V virus and between random intranuclear positions and NE in CEM-SS cells expressing Bgl-mCherry. For (B) and (D), statistical significance was determined using Kolmogorov-Smirnov tests. ****, $P < 0.0001$; *, $P < 0.05$; ns, not significant ($P > 0.05$).

prior to uncoating, HeLa cells were infected with HIV-1 virions labeled with a mCherry fluid-phase marker, similar to labeling viral cores with a GFP fluid-phase marker as recently reported by us and others (10, 46, 47). Briefly, infectious mCherry-labeled HIV-1 virions were generated using a modified HIV-1 Gag-pol vector containing an mCherry that was inserted between matrix (MA) and CA and complementation with WT Gag-pol (1:2 ratio) to generate infectious virions. During virion maturation, mCherry is fully processed by HIV-1 protease;
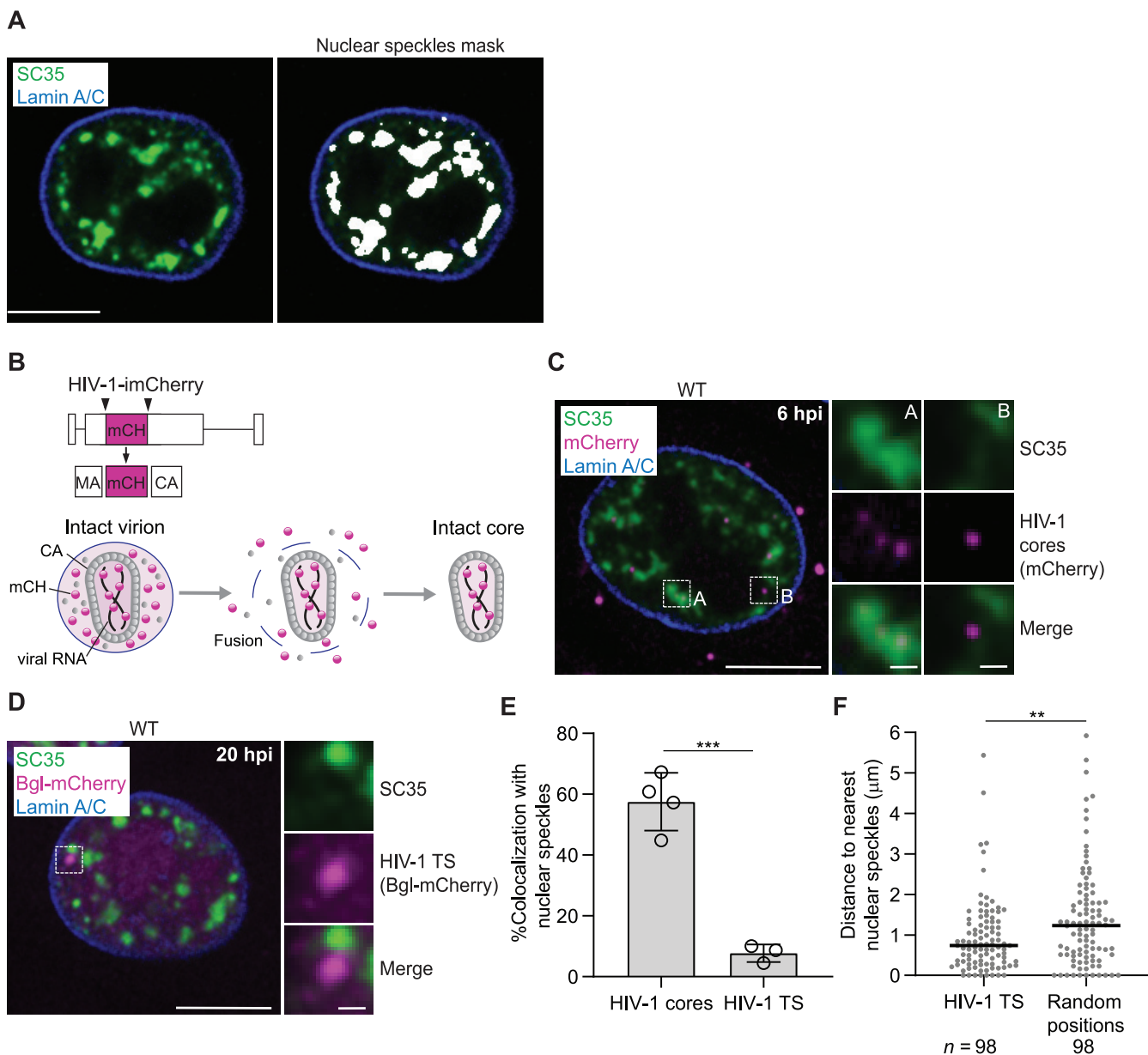
FIG 6 Detection of HIV-1 cores, but not HIV-1 TS, in nuclear speckles (A) The SC35 immunostaining signal (left; green) was used to generate a mask of the nuclear speckles (right) using a custom MATLAB program. Scale bar, 10 μm. (B) HIV-1 vector used to generate mCherry-labeled HIV-1 virions (top panel). mCherry is a fluid-phase marker that can be used to detect intact HIV-1 cores after fusion of the viral and cell membranes (bottom panel). (C) Detection of HIV-1 cores and nuclear speckles in HeLa cells 6 hpi. HeLa cells were infected with mCherry-labeled HIV-1 virions, fixed at 6 hpi, and then nuclear speckles were analyzed by indirect immunostaining of SC35. Three HIV-1 cores that colocalize with SC35 signal (panel A) and an HIV-1 core that does not colocalize with SC35 signal (panel B). (D) Detection of HIV-1 TS and nuclear speckles in HeLa cells 20 hpi. HeLa cells expressing Bgl-mCherry were infected with HIV-1 containing BglSL, fixed at 20 hpi, and then nuclear speckles were visualized by immunostaining of SC35. Panel shows HIV-1 TS that does not colocalize with SC35 signal. For (C) and (D), scale bar, 10 μm; inset scale bar, 1 μm. (E) The percentage of HIV-1 cores and HIV-1 TS that colocalize with nuclear speckles from four and three independent experiments (open circles), respectively. A total of 2,679 HIV-1 cores and 98 HIV-1 TS were analyzed. Statistical significance was determined using a Welch's t test; ***, $P < 0.001$. (F) The distance between HIV-1 TS or random positions inside the nucleus to nuclear speckles. Statistical significance was determined using a Mann-Whitney test; **, $P < 0.01$.

some mCherry is trapped between the viral membrane and the mature viral core and some mCherry is trapped within the mature viral core (Fig. 6B). Viral cores labeled with mCherry were detected inside the infected cell nuclei at 6 hpi (Fig. 6C), consistent with our previous observation that viral cores labeled with a GFP fluid-phase marker could be readily detected in infected cell nuclei (10). To identify HIV-1 TSs, HeLa cells expressing Bgl-mCherry were infected with HIV-1 virions containing BglSL and HIV-1 TSs were detected at 20 hpi (Fig. 6D). A majority of nuclear HIV-1 cores (57.6%) colocalized with nuclear speckles. These results are

consistent with recent observations that HIV-1 RTCs/PICs frequently colocalized with nuclear speckles (12, 15). However, very few active proviruses (7.6%) colocalized with nuclear speckles (Fig. 6E). The average distance between active proviruses and the nearest nuclear speckle (~0.9 μm) was smaller than the average distance between random positions and the nearest nuclear speckle (~1.4 μm). Thus, consistent with recent reports (12, 48), the results indicated that active proviruses are located closer to nuclear speckles than would be expected if the proviruses were randomly distributed in the nucleus (Fig. 6F). In summary, these findings indicate that although viral cores localize to nuclear speckles prior to uncoating, active proviruses are located adjacent to nuclear speckles.

DISCUSSION

Determining the intranuclear positions of active proviruses may provide insight into how HIV-1 selects suitable genomic targets for integration and the relationship between the position of proviruses in the cell nucleus and their transcription activity. Here, we observed that the transcriptional activity of proviruses was not correlated with their radial positioning inside the nucleus at early (24 hpi) or late (5 dpi) time points. Our results showed that active proviruses are positioned near the nuclear periphery shortly after infection, and that host factors LEDGF/p75 and CPSF6 have different effects on the nuclear positioning and transcriptional activity of proviruses. In LEDGF/p75-depleted HeLa cells, the radial position of active proviruses was not altered, but their transcription activity was significantly reduced, whereas when capsid-CPSF6 interaction was disrupted by CA mutations, the radial position of active proviruses in HeLa cells was much closer to the NE but their transcriptional activity was not significantly altered. Taken together, these results indicate that the local chromatin environment of the proviruses, but not their radial nuclear positioning, is likely to provide greater insight into the regulation of HIV-1 transcription and the mechanism of HIV-1 latency.

We detected active proviruses using two different methods that have their own advantages and limitations. The RNA stem-loop technology is suitable for live-cell imaging to determine the dynamics of HIV-1 transcription from single proviruses but requires the insertion of multiple RNA stem loops in the viral genome. RNAscope can be used to detect WT HIV-1 genomes but is limited to fixed cells and requires extensive sample processing, which can perturb cell morphology. One caveat of these two detection methods is that we could not determine the positions of transcriptionally inactive proviruses, which may be different than the positions of active proviruses. However, our previously published observations argue against the hypothesis that the intranuclear positions of transcriptionally inactive and active proviruses at 24 hpi are different. We previously showed that viral cores labeled with fluorescent proteins are localized ~1.4 μm from the NE at 6 hpi (17, 21). Furthermore, the viral cores remain at these locations for several hours, uncoat, and the released vDNA integrates into nearby chromatin (1), indicating that the distribution of all integration sites is likely to be similar to that of viral cores at 6 hpi. Finally, the distribution of active proviruses is similar to that of viral cores at 6 hpi (1). Since the distribution of viral cores is similar to the distribution of all integration sites and the distribution of active proviruses, we believe the distribution of inactive proviruses is not likely to be different from that of active proviruses. We also previously observed that the viral cores in the nuclei of LEDGF/p75 KO cells were on average located the same distance from the NE as in unmodified HeLa cells (21). Since integrations occur close the locations of the viral cores (1), we believe the data suggest that LEDGF/p75 KO did not significantly alter the locations of integrations but did reduce the level of HIV-1 transcription from infected cells (cells expressing HIV-1 RNA).

Interestingly, in contrast to HeLa cells, there was little or no change in the radial positioning of active proviruses in CEM-SS cells after disruption of the CA-CPSF6 interaction. Although the proviruses derived from the N74D mutant were ~50 nm closer to the NE than WT proviruses ($P < 0.05$), the proviruses derived from the A77V mutant were not significantly different from WT with respect to the distance from the NE ($P > 0.05$). These observations suggest that the preferred sites of integration in CEM-SS cells for the WT and CPSF6-binding-defective active proviruses were located a similar distance away from the NE. Whether this difference between HeLa and CEM-SS cells is due to differences in chromatin organization or

nucleus size is unclear at this time. In addition, the disruption of the CA-CPSF6 interaction did not have a detectable effect on the level of HIV-1 transcription even though integration primarily occurs in or near LADs (7, 8), which are regions of chromosomes typically associated with lower gene expression (reviewed in reference 49). These results suggest that, in the absence of CA-CPSF6 interaction, HIV-1 integrates into the transcriptionally active chromatin areas of LADs, presumably in a LEDGF/p75-dependent manner. Alternatively, HIV-1 integrates in the repressive chromatin within LADs but can somehow overcome the suppression of the chromatin environment near the proviruses. Nevertheless, the similar levels of transcriptional activity of mutant and WT proviruses are consistent with their similar infectivities (1, 40).

We previously estimated that only a small number of RTCs/PICs enter the nucleus, indicating that nuclear import is a major block to infection (17, 21). Here, we estimate that only 1 in ~7 vDNAs inside the nucleus will lead to productive infection, indicating that only a fraction of RTCs/PICs that initiate reverse transcription and enter the nucleus lead to productive infection. Indeed, not all vDNAs inside the nucleus are expected to integrate, since unintegrated forms of HIV-1 DNA such as linear DNA and 1- or 2-long terminal repeat circles can be readily detected (reviewed in reference 30). Other possibilities for the failure of the viruses to lead to productive infection include a defect in nuclear HIV-1 core uncoating (1), incomplete DNA synthesis (incomplete RT products of sufficient size would be detected in the highly sensitive *in situ* hybridization assay), failure to integrate, or integration into regions of the genome that are not conducive to HIV-1 gene expression.

Some studies have reported a pan-nuclear distribution of vDNA (6, 9), while other studies have reported peripheral distribution (16, 23, 25). The different interpretations are likely due to differences between the methods used to analyze the results. In some studies, the nucleus was partitioned into three zones of roughly equal area and then the colocalization of vDNA foci within these zones was determined. In these studies, transcriptionally active and inactive integrated and unintegrated vDNA were examined, whereas in our studies, only transcriptionally active integrated vDNA was analyzed. In addition, the fact that nuclei are not perfect spheres, the number of zones chosen, and subtle differences in the way the zones are defined (6, 9, 50) could lead to different interpretation of the results. Here, like some other studies (16, 20, 23, 29), we compared the distances between the proviruses and the nucleus boundary directly to the distances obtained from random positions inside the nucleus; therefore, we were able to determine if the proviruses are closer to the NE than would be expected by random chance. We previously observed that after entering the nucleus HIV-1 cores do not move far from their point of nuclear entry (~2.3 μm), remain near the NE (~1.4 μm), and that their movement is significantly restricted and indistinguishable from the restricted movement of genes (21), indicating the vDNA integrates into chromatin that is located near the point of nuclear entry.

Previous genome-wide HIV-1 integration site studies have shown that a large proportion of actively transcribed genes are targeted by HIV-1 for integration (51, 52). Our results indicate that HIV-1 prefers to integrate into genes that are located near the nuclear periphery at the time of infection, but the locations of these genes change as a result of cell division. Our observation that gene positions are dynamic is consistent with previous studies showing that gene positions vary substantially from cell to cell (38, 53). Thus, although HIV-1 prefers to integrate into genes that are located near the nuclear periphery, the dynamic nature of genes in a large population of cells allows for most of the genomic sites of integration to be located at this preferred distance from the NE in some infected cells.

We observed that most HIV-1 cores inside the nucleus colocalize with nuclear speckles but that most HIV-1 TSs do not. It is important to note that our previous results suggest that HIV-1 TSs become detectable several hours after integration (1). Therefore, the active provirus could have separated from the nuclear speckles between integration and TS detection. Alternatively, it is possible that uncoating occurs within nuclear speckles but that integration occurs in genes located adjacent to nuclear speckles; the low density of genes in this interchromatin space relative to other regions of the nucleus (reviewed in reference 13) and the absence of transcribing genes inside nuclear speckles (54) may result in few targets available for integration inside nuclear speckles. Given the dynamic nature of nuclear speckles, HIV-1

cores and/or the PICs released from the capsids may exit the nuclear speckle and integrate into the nearby chromatin. Future studies will be required to further elucidate the role of nuclear speckles in uncoating, integration site selection, and transcription.

Overall, these studies support a model in which WT viral cores enter the nucleus and penetrate to an average distance of ~1.4 μm, uncoat and integrate into nearby sites in a LEDGF/p75-dependent manner. The results of these studies also explain the seemingly paradoxical observations that the preferred sites of integration are located near the nuclear periphery, and yet genome-wide integration site analysis shows that HIV-1 integrates throughout the human genome (51, 52). The observation that the locations of active proviruses become random after a few cell divisions indicates that the subset of genes located at the ~1.4 μm distance from the NE are different in each cell, and that the entire genome is available for HIV-1 integration at this preferred penetration distance in a population of cells. It has been suggested that CPSF6 plays a role in localizing the viral core to nuclear speckles near the sites of integration (9, 12); other unidentified host factors may also facilitate viral core localization near sites of integration as well as the selection of chromosomal sites for integration by the PIC after its release from the capsid. These studies also show that the distance from the NE to the integration site is cell-type dependent and does not correlate with proviral transcription activity. Thus, the local chromatin organization, and not the radial positioning of proviruses, has a greater influence on proviral transcription activity. Identification of intact proviruses from elite controllers that were integrated into genomic regions containing centromeric satellite DNA and other heterochromatic regions (55) strongly suggests that selection of integration sites that enable proviral transcription is an essential step in HIV-1 replication.

MATERIALS AND METHODS

Cell lines and reagents. HeLa (American Type Culture Collection [ATCC CCL-2]), HeLa:LEDGF/p75 knockout (LKO) (21), and Human embryonic kidney 293T cells (ATCC CRL-3216) were maintained as previously described. CEM-SS cells (NIH AIDS Reagent Program, Division of AIDS, NIAID, NIH; gift from Dr. Peter L. Nara; Catnumber 776) were maintained in Roswell Park Memorial Institute (RPMI) 1640 medium (CellGro, Manassas, VA) supplemented with 10% fetal calf serum (HyClone, Logan, UT) and 1% penicillin-streptomycin (penicillin 50 U/ml and streptomycin 50 μg/ml; Lonza, Walkersville, MD). To generate the CEM-SS:Bgl-mCherry cell line, CEM-SS cells were transduced with the lentiviral vector pLVX-TRE3G-Bgl-mCherry (1), which expresses a truncated bacterial protein BglG that is fused to mCherry at the C terminus and contains a nuclear localization signal (Bgl-mCherry) from a doxycycline-inducible promoter, and Tet-On 3G (Clontech, Mountainview, CA), which expresses the transactivator protein. The transduced cells are maintained in complete media containing puromycin (0.5 μg/ml; Thermo Fisher Scientific) and G418 Sulfate (200 μg/ml; Sigma-Aldrich). Doxycycline (Sigma-Aldrich; 1 μg/ml) was added for 24 h prior to imaging to induce Bgl-mCherry expression. Aphidicolin (Abcam, Waltham, MA, Cat. number 142400) was used at a final concentration of 10 μg/ml. NVP and RAL were obtained through the NIH AIDS Reagent Program and were used at final concentrations of 5 μM and 10 μM, respectively.

HIV-1 constructs and infections. HIV-1 particles were prepared by cotransfection of 293T cells with the HIV-1-derived replication-defective vector pHDV-EGFP kindly provided by Derya Unutmaz (New York University) (56), which is deficient for envelope glycoprotein gene (*env*) and the accessory genes *vif*, *vpr*, *vpu*, and *nef*, and can only complete a single cycle of replication. HCMV-G (57), which expresses the G glycoprotein of vesicular stomatitis virus (VSV-G), was used to produce VSV-G-pseudotyped HIV-1 particles. In some instances, 293T cell lines generated by transduction with pHDV-EGFP were transfected with HCMV-G to generate VSV-G pseudotyped HIV-1 particles. The HIV-1 derived vectors pHGFP-BglSL, pHGFP(N74D)-BglSL, and pHGFP(A77V)-BglSL, which are HIV-1 vectors containing either WT CA, N74D CA, or A77V CA and express a *gfp* reporter gene (in place of *nef*) and contain BglSL in place of *vif/vpr* were previously described (1). HIV-1 virions labeled with mCherry fluid-phase marker were prepared by cotransfection of 293T cells with HIV Gag-imCherry, which is a vector that was created by replacing the GFP in HIV Gag-iGFP [NIH AIDS Reagent Program, Division of AIDS, NIAID, NIH: gift from Dr. Benjamin Chen; Catnumber 12457] with mCherry, and pH-GFP (1), which is an HIV-1 vector that contains a *gfp* reporter gene and does not express *env*, at a 1:2 ratio. For DNAscope and RNAscope, HeLa cells (3 × 10⁴) were seeded onto Lab-Tek II CC2 8-well chambered slides (VWR; Cat. number 62407-025) the day before infection and virus was added directly to the cells. For immunostaining experiments, HeLa cells (3 × 10⁴) were seeded onto ibiTreated μ-slides (Ibidi) the day before infection and virus was added directly to the cells. The CEM-SS:Bgl-mCherry cells were seeded into ibiTreated μ-slides (100,000 cells/well) that were pretreated with poly-L-lysine (Sigma-Aldrich; Cat.number P8920).

To determine virus infectivity, cells were infected with titrations of *gfp* reporter virus, fixed at 48 h postinfection with 2% paraformaldehyde (PFA in 1X PBS), and the percentage of GFP⁺ cells was determined by flow cytometry. For RNAscope, cells were infected with an HIV-1-derived GFP reporter virus at

a multiplicity of infection (MOI) of 0.05 (~5% GFP positive cells 48 hpi). For DNAscope (described below), cells were infected with an HIV-1-derived GFP reporter virus at an MOI of 0.3 (~30% GFP positive cells 48 hpi). The infected cells were fixed with 10% neutral buffered formalin (NBF) for 30 min at room temperature (RT). The NBF was removed and the chamber was carefully removed, leaving the fixed cells on the microscope slide. Cells were dehydrated and permeabilized by successive treatments of increasing Ethanol (EtOH) (50% EtOH for 5 min at RT, 70% EtOH for 5 min at RT, then 100% EtOH for 5 min at RT). The slides (in 100% EtOH) were stored at −20°C or processed immediately.

Detection of HIV-1 and GAPDH RNA using RNAscope. To detect HIV-1 RNA, the RNAscope Fluorescence Multiplex reagent kit (Advanced Cell Diagnostics, Inc.; Cat. number 320850) was used, with some modifications. The slides were rehydrated in 70% EtOH for 2 min at RT, 50% EtOH for 2 min at RT, and in 1X phosphate-buffered saline (PBS) for 10 min at RT. For some experiments, the cells were fixed with 4% PFA (in 1X PBS) for 10 min at RT or 10% NBF for 30 min at RT followed by permeabilization with 0.25% TritonX-100 in 1X PBS for 10 min at RT. The cells were pretreated with Protease III (1:15 dilution in 1X PBS) for 10 min at RT, then rinsed 2X in 1X PBS. For detection of HIV-1 RNA, cells were incubated with probe V-HIV1-CladeB (Cat. number 416111;78 pairs of "double-Z" probes that target regions 854–8291 of pNL4-3 sequence [GenBank: AF324493.2]) diluted 1:3 in blank buffer for 2 h at 40°C, followed by 2 × 2 min washes in 1X Wash Buffer. For detection of GAPDH RNA, cells were incubated with probe Hs-GAPDH (Cat. number 310321) diluted 1:3 in blank buffer for 2 h at 40°C, followed by 2 × 2 min washes in 1X Wash Buffer. For signal amplification, samples were treated with Amplification Probe-1 (Amp-1) for 30 min at 40°C (followed by 2 × 2 min in 1X Wash Buffer), Amp-2 for 15 min at 40°C (followed by 2 × 2 min in 1X Wash Buffer), Amp-3 for 30 min at 40°C (followed by 2 × 2 min in 1X Wash Buffer), and Amp-4 for 15 min at 40°C (followed by 2 × 2 min in 1X Wash Buffer). The cells were counterstained with DAPI for 30 sec at RT. A number 1.5 coverslip was mounted to the slides using ProLong Gold Antifade Mountant (ThermoFisher; Cat. number P36930) and the coverslip was sealed using nail lacquer. The samples were stored in the dark at 4°C until imaging.

Detection of HIV-1 DNA using DNAscope. To detect HIV-1 DNA, the RNAscope 2.5 HD reagent kit-Brown (Advanced Cell Diagnostics, Inc.; Cat. number 322300) was used (33), with some modifications. After rehydration, samples were treated with hydrogen peroxide for 10 min at RT (followed by 2 × 2 min in distilled H_2O [dH$_2$0]), boiled in 1X Target Retrieval Reagent for 30 min (followed by 2 × 2 min in dH$_2$0), and treated with Protease III (1:5 dilution in 1X PBS) for 15 min at 40°C (followed by 2 × 2 min in dH$_2$0). For hybridization, the cells were incubated with probe V-HIV1-CladeB-sense (Cat. number 425531; probes that are the anti-sense of the probes used to detect HIV-1 RNA) for 18 h at 40°C, followed by 2 × 2 min washes in 0.5X Wash Buffer. For signal amplification, samples were treated with 2.5 HD Amp-1 for 30 min at 40°C (followed by 2 × 2 min in 0.5X Wash Buffer), 2.5 HD Amp-2 for 15 min at 40°C (followed by 2 × 2 min in 0.5X Wash Buffer), 2.5 HD Amp-3 for 30 min at 40°C (followed by 2 × 2 min in 0.5X Wash Buffer), 2.5 HD Amp-4 for 15 min at 40°C (followed by 2 × 2 min in 0.5X Wash Buffer), 2.5 HD Amp-5 for 30 min at RT (followed by 2 × 2 min in 0.5X Wash Buffer), and 2.5 HD Amp-6 for 15 min at RT (followed by 2 × 2 min in 0.5X Wash Buffer). The samples were placed in Tris Buffered Saline + Tween 20 (0.05% vol/vol; TBS-Tween) immediately before development. The samples were incubated with a tyramide signal amplification (TSA) Plus Cyanine 3.5 working solution (1:1000 TSA stock solution in 1X amplification diluent; Perkin-Elmer) for 5 min at RT and plunged in 0.5X Wash Buffer to stop the reaction. A final wash with 1X TBS-Tween and then 1X PBS. The cells were counterstained with DAPI for 30 sec at RT. A number 1.5 coverslip was mounted to the slides using ProLong Gold Antifade Mountant and the coverslip was sealed using nail lacquer. The samples were stored in the dark at 4°C until imaging.

Simultaneous detection of HIV-1 RNA and DNA. The HIV-1 DNA was first detected using the DNAscope assay described above up to the step of the final wash in 1X PBS. Then, HIV-1 RNA was detected using the RNAscope assay described above, except that probe V-HIV1-CladeB-C3 (Cat. number 416111-C3) was used. The cells were counterstained with DAPI for 30 sec at RT. A number 1.5 coverslip was mounted to the slides using Prolong Gold Mount and the coverslip was sealed using nail lacquer. The samples were stored in the dark at 4°C until imaging.

Detection of nuclear speckles. Nuclear speckles were identified by indirect immunostaining of SC35, a protein that is highly enriched in nuclear speckles (reviewed in reference 13). Cells were fixed with 4% PFA for 10 min at RT and permeabilized using 1X PBS + 0.25% TX-100 for 10 min at RT (followed by 2 × 2 min in Immunofluorescence Staining Wash Buffer [IWB; 1X PBS + 0.1% TX-100]). For blocking, cells were incubated with IWB + 3% bovine serum albumin (BSA; Sigma-Aldrich; Cat. number A7638) for 1 h at RT. Cells were incubated with mouse anti-SC35 antibody diluted 1:1000 in IWB + 1% BSA (Sigma-Aldrich; Cat. number S4045) and rabbit anti-Lamin A/C diluted 1:1000 in IWB + 1% BSA (Sigma-Aldrich; Cat. number L1293) for 1 h at RT (followed by 3 × 2 min washes in IWB + 1% BSA). For detection, cells were incubated with anti-rabbit AlexaFluor405-conjugated secondary antibody diluted 1:1000 in IWB + 1% BSA (ThermoFisher; Cat. number A-31556) and anti-mouse AlexaFluor488-conjugated secondary antibody diluted in 1:1000 in IWB + 1% BSA (ThermoFisher, Cat. number A-11001) for 1 h at RT (followed by 3 × 2 min washes in IWB + 1% BSA). Cells were stored in 1X PBS and imaged immediately or the next day.

Microscopy and image processing. Confocal z-stacks of the infected cells (~34 slices with 0.2 μm step size) were acquired using either a LSM710 laser scanning confocal microscope (Zeiss) equipped with 405-nm (DAPI), 488-nm (FITC/GFP), and 561-nm (Cy3.5) lasers for illumination and a Plan-Apochromat 63x NA-1.40 oil objective or a Nikon Eclipse T*i*-E microscope equipped with a Yokogawa CSU-X1 spinning disk unit and 405-nm (DAPI), 488-nm (FITC/GFP), and 594-nm (mCherry) lasers for illumination, and a Plan-Apochromat 100x N.A. 1.49 oil objective. Images were captured on the Nikon microscope using a TwinCam system (Cairn, Faversham, UK) equipped with a 565-nm splitter and two iXon Ultra (Andor, Belfast, UK) cameras. The Nikon microscope was also equipped with a Tokai Hit microscope stage top incubator (Tokai, Japan) and was used for all live-cell imaging experiments. Images of the infected cells were examined using Nikon Elements, ZEN

lite, or ImageJ. For display, a pixel-averaging filter was applied to the images and the contrast was adjusted; unmodified images were used for intensity analyses.

The distance between the HIV-1 TS and the nucleus boundary (i.e., NE) was determined using a custom MATLAB program. Briefly, the HIV-1 TSs were first identified manually and then their x, y and z positions were further refined by three-dimensional gaussian fitting. The three-dimensional nucleus boundary was determined using the DAPI or diffuse Bgl-mCherry signal (Bgl-mCherry contains a nuclear localization signal; thus, most of the Bgl-mCherry localized inside the nucleus) using the confocal z-slices. The three-dimensional distance between the HIV-1 TS and the nearest point at the nucleus boundary was determined. To determine the distance between random positions inside the nucleus and the NE, random coordinates (x, y and z) were generated using a custom MATLAB program and the three-dimensional distance between each random position inside the nucleus and the nearest point at the nucleus boundary was determined. If the proviruses were randomly distributed in the nucleus, the distances between the proviruses and the NE would be similar to the distances between random positions and the NE. Cumulative frequency distributions were used to analyze the distances between the HIV-1 TS (or random positions inside the nucleus) and the NE. The local background-subtracted pixel intensities of the HIV-1 TS were determined.

To determine colocalization of HIV-1 cores labeled with mCherry content marker and HIV-1 TS with nuclear speckles, a mask of the nuclear speckles was first generated using the SC35 immunostaining signal (Fig. 6A). Next, the positions of the HIV-1 cores or HIV-1 TS were used to determine colocalization with the nuclear speckles mask. To determine the distance between random positions inside the nucleus and nuclear speckles, random coordinates (x, y) were generated using a custom MATLAB program. Next, the two-dimensional distance between each random position inside the nucleus and the nearest nuclear speckle boundary was determined.

To determine the level of photobleaching of the Alexa Fluor 488-labeled probes, 15 z-stacks (34 images/z-stack with 0.2-μm step size) were consecutively acquired of infected cells that had been fixed 24 hpi and stained for HIV-1 RNA using RNAscope. The HIV-1 TS fluorescence intensity was determined for 10 different HIV-1 TSs (Fig. S2). The results indicated that photobleaching of Alexa Fluor 488-labeled probes was minimal for a single z-stack and was only detectable after the 3rd z-stack (8% decrease in fluorescence intensity from 1st z-stack to 4th z-stack; $P = 0.0374$). Importantly, fluorescence intensities of TSs were determined using images of cells that had been acquired using a single z-stack; therefore, the fluorescence intensities of samples were minimally affected by photobleaching.

Statistics. The Welch's unpaired t test and paired t test were used to analyze parametric data. The Mann-Whitney U test was used to analyze nonparametric data and the Kolmogorov-Smirnov test was used to analyze cumulative frequencies. A Fisher's exact test was used to analyze 2 × 2 contingency tables. All statistical tests were performed in Prism 8 (GraphPad Software, San Diego, CA). P values $<$ 0.05 were considered significant.

SUPPLEMENTAL MATERIAL

Supplemental material is available online only.

FIG S1, EPS file, 0.5 MB.

FIG S2, EPS file, 0.6 MB.

ACKNOWLEDGMENTS

REFERENCES

1. Burdick RC, Li C, Munshi M, Rawson JMO, Nagashima K, Hu WS, Pathak VK. 2020. HIV-1 uncoats in the nucleus near sites of integration. Proc Natl Acad Sci U S A 117:5486–5493. https://doi.org/10.1073/pnas.1920631117.

2. Cherepanov P, Maertens G, Proost P, Devreese B, Van Beeumen J, Engelborghs Y, De Clercq E, Debyser Z. 2003. HIV-1 integrase forms stable tetramers and associates with LEDGF/p75 protein in human cells. J Biol Chem 278:372–381. https://doi.org/10.1074/jbc.M209278200.

3. Maertens G, Cherepanov P, Pluymers W, Busschots K, De Clercq E, Debyser Z, Engelborghs Y. 2003. LEDGF/p75 is essential for nuclear and chromosomal targeting of HIV-1 integrase in human cells. J Biol Chem 278:33528–33539. https://doi.org/10.1074/jbc.M303594200.

4. Singh PK, Plumb MR, Ferris AL, Iben JR, Wu X, Fadel HJ, Luke BT, Esnault C, Poeschla EM, Hughes SH, Kvaratskhelia M, Levin HL. 2015. LEDGF/p75 interacts with mRNA splicing factors and targets HIV-1 integration to highly spliced genes. Genes Dev 29:2287–2297. https://doi.org/10.1101/gad.267609.115.

5. Lee K, Ambrose Z, Martin TD, Oztop I, Mulky A, Julias JG, Vandegraaff N, Baumann JG, Wang R, Yuen W, Takemura T, Shelton K, Taniuchi I, Li Y, Sodroski J, Littman DR, Coffin JM, Hughes SH, Unutmaz D, Engelman A, KewalRamani VN. 2010. Flexible use of nuclear import pathways by HIV-1. Cell Host Microbe 7:221–233. https://doi.org/10.1016/j.chom.2010.02.007.

6. Chin CR, Perreira JM, Savidis G, Portmann JM, Aker AM, Feeley EM, Smith MC, Brass AL. 2015. Direct Visualization of HIV-1 replication intermediates

shows that capsid and CPSF6 modulate HIV-1 intra-nuclear invasion and integration. Cell Rep 13:1717–1731. https://doi.org/10.1016/j.celrep.2015.10.036.

7. Sowd GA, Serrao E, Wang H, Wang W, Fadel HJ, Poeschla EM, Engelman AN. 2016. A critical role for alternative polyadenylation factor CPSF6 in targeting HIV-1 integration to transcriptionally active chromatin. Proc Natl Acad Sci U S A 113:E1054–E1063. https://doi.org/10.1073/pnas.1524213113.

8. Schaller T, Ocwieja KE, Rasaiyaah J, Price AJ, Brady TL, Roth SL, Hue S, Fletcher AJ, Lee K, KewalRamani VN, Noursadeghi M, Jenner RG, James LC, Bushman FD, Towers GJ. 2011. HIV-1 capsid-cyclophilin interactions determine nuclear import pathway, integration targeting and replication efficiency. PLoS Pathog 7:e1002439. https://doi.org/10.1371/journal.ppat.1002439.

9. Achuthan V, Perreira JM, Sowd GA, Puray-Chavez M, McDougall WM, Paulucci-Holthauzen A, Wu X, Fadel HJ, Poeschla EM, Multani AS, Hughes SH, Sarafianos SG, Brass AL, Engelman AN. 2018. Capsid-CPSF6 interaction licenses nuclear HIV-1 trafficking to sites of viral DNA integration. Cell Host Microbe 24:392–404. https://doi.org/10.1016/j.chom.2018.08.002.

10. Li C, Burdick RC, Nagashima K, Hu WS, Pathak VK. 2021. HIV-1 cores retain their integrity until minutes before uncoating in the nucleus. Proc Natl Acad Sci U S A 118.

11. Guelen L, Pagie L, Brasset E, Meuleman W, Faza MB, Talhout W, Eussen BH, de Klein A, Wessels L, de Laat W, van Steensel B. 2008. Domain organization of human chromosomes revealed by mapping of nuclear lamina interactions. Nature 453:948–951. https://doi.org/10.1038/nature06947.

12. Francis AC, Marin M, Singh PK, Achuthan V, Prellberg MJ, Palermino-Rowland K, Lan S, Tedbury PR, Sarafianos SG, Engelman AN, Melikyan GB. 2020. HIV-1 replication complexes accumulate in nuclear speckles and integrate into speckle-associated genomic domains. Nat Commun 11: 3505. https://doi.org/10.1038/s41467-020-17256-8.

13. Spector DL, Lamond AI. 2011. Nuclear speckles. Cold Spring Harb Perspect Biol 3. https://doi.org/10.1101/cshperspect.a000646.

14. Thiry M. 1995. The interchromatin granules. Histol Histopathol 10:1035–1045.

15. Rensen E, Mueller F, Scoca V, Parmar JJ, Souque P, Zimmer C, Di Nunzio F. 2021. Clustering and reverse transcription of HIV-1 genomes in nuclear niches of macrophages. EMBO J 40:e105247. https://doi.org/10.15252/embj.2020105247.

16. Albanese A, Arosio D, Terreni M, Cereseto A. 2008. HIV-1 pre-integration complexes selectively target decondensed chromatin in the nuclear periphery. PLoS One 3:e2413. https://doi.org/10.1371/journal.pone.0002413.

17. Burdick RC, Hu WS, Pathak VK. 2013. Nuclear import of APOBEC3F-labeled HIV-1 preintegration complexes. Proc Natl Acad Sci U S A 110:E4780–E4789. https://doi.org/10.1073/pnas.1315996110.

18. Francis AC, Melikyan GB. 2018. Single HIV-1 imaging reveals progression of infection through CA-dependent steps of docking at the nuclear pore, uncoating, and nuclear transport. Cell Host Microbe 23:536–548. https://doi.org/10.1016/j.chom.2018.03.009.

19. Zurnic Bonisch I, Dirix L, Lemmens V, Borrenberghs D, De Wit F, Vernaillen F, Rocha S, Christ F, Hendrix J, Hofkens J, Debyser Z. 2020. Capsid-labelled HIV to investigate the role of capsid during nuclear import and integration. J Virol 94. https://doi.org/10.1128/JVI.01024-19.

20. Quercioli V, Di Primio C, Casini A, Mulder LCF, Vranckx LS, Borrenberghs D, Gijsbers R, Debyser Z, Cereseto A. 2016. Comparative analysis of HIV-1 and murine leukemia virus three-dimensional nuclear distributions. J Virol 90:5205–5209. https://doi.org/10.1128/JVI.03188-15.

21. Burdick RC, Delviks-Frankenberry KA, Chen J, Janaka SK, Sastri J, Hu WS, Pathak VK. 2017. Dynamics and regulation of nuclear import and nuclear movements of HIV-1 complexes. PLoS Pathog 13:e1006570. https://doi.org/10.1371/journal.ppat.1006570.

22. Hulme AE, Perez O, Hope TJ. 2011. Complementary assays reveal a relationship between HIV-1 uncoating and reverse transcription. Proc Natl Acad Sci U S A 108:9975–9980. https://doi.org/10.1073/pnas.1014522108.

23. Di Primio C, Quercioli V, Allouch A, Gijsbers R, Christ F, Debyser Z, Arosio D, Cereseto A. 2013. Single-cell imaging of HIV-1 provirus (SCIP). Proc Natl Acad Sci U S A 110:5636–5641. https://doi.org/10.1073/pnas.1216254110.

24. Puray-Chavez M, Tedbury PR, Huber AD, Ukah OB, Yapo V, Liu D, Ji J, Wolf JJ, Engelman AN, Sarafianos SG. 2017. Multiplex single-cell visualization of nucleic acids and protein during HIV infection. Nat Commun 8:1882. https://doi.org/10.1038/s41467-017-01693-z.

25. Marini B, Kertesz-Farkas A, Ali H, Lucic B, Lisek K, Manganaro L, Pongor S, Luzzati R, Recchia A, Mavilio F, Giacca M, Lusic M. 2015. Nuclear architecture dictates HIV-1 integration site selection. Nature 521:227–231. https://doi.org/10.1038/nature14226.

26. Peng K, Muranyi W, Glass B, Laketa V, Yant SR, Tsai L, Cihlar T, Muller B, Krausslich HG. 2014. Quantitative microscopy of functional HIV post-entry complexes reveals association of replication with the viral capsid. Elife 3: e04114. https://doi.org/10.7554/eLife.04114.

27. De Wit F, Pillalamarri SR, Sebastian-Martin A, Venkatesham A, Van Aerschot A, Debyser Z. 2019. Design of reverse transcriptase-specific nucleosides to visualize early steps of HIV-1 replication by click labeling. J Biol Chem 294:11863–11875. https://doi.org/10.1074/jbc.RA118.007185.

28. Bejarano DA, Peng K, Laketa V, Borner K, Jost KL, Lucic B, Glass B, Lusic M, Muller B, Krausslich HG. 2019. HIV-1 nuclear import in macrophages is regulated by CPSF6-capsid interactions at the nuclear pore complex. Elife 8. https://doi.org/10.7554/eLife.41800.

29. Vranckx LS, Demeulemeester J, Saleh S, Boll A, Vansant G, Schrijvers R, Weydert C, Battivelli E, Verdin E, Cereseto A, Christ F, Gijsbers R, Debyser Z. 2016. LEDGIN-mediated Inhibition of Integrase-LEDGF/p75 Interaction Reduces Reactivation of Residual Latent HIV. EBioMedicine 8:248–264. https://doi.org/10.1016/j.ebiom.2016.04.039.

30. Hamid FB, Kim J, Shin CG. 2017. Distribution and fate of HIV-1 unintegrated DNA species: a comprehensive update. AIDS Res Ther 14:9. https://doi.org/10.1186/s12981-016-0127-6.

31. Zhu Y, Wang GZ, Cingoz O, Goff SP. 2018. NP220 mediates silencing of unintegrated retroviral DNA. Nature 564:278–282. https://doi.org/10.1038/s41586-018-0750-6.

32. Geis FK, Goff SP. 2019. Unintegrated HIV-1 DNAs are loaded with core and linker histones and transcriptionally silenced. Proc Natl Acad Sci U S A 116:23735–23742. https://doi.org/10.1073/pnas.1912638116.

33. Deleage C, Wietgrefe SW, Del Prete G, Morcock DR, Hao XP, Piatak M, Jr, Bess J, Anderson JL, Perkey KE, Reilly C, McCune JM, Haase AT, Lifson JD, Schacker TW, Estes JD. 2016. Defining HIV and SIV reservoirs in lymphoid tissues. Pathog Immun 1:68–106. https://doi.org/10.20411/pai.v1i1.100.

34. Chen J, Nikolaitchik O, Singh J, Wright A, Bencsics CE, Coffin JM, Ni N, Lockett S, Pathak VK, Hu WS. 2009. High efficiency of HIV-1 genomic RNA packaging and heterozygote formation revealed by single virion analysis. Proc Natl Acad Sci U S A 106:13535–13540. https://doi.org/10.1073/pnas.0906822106.

35. Hansen MMK, Wen WY, Ingerman E, Razooky BS, Thompson CE, Dar RD, Chin CW, Simpson ML, Weinberger LS. 2018. A post-transcriptional feedback mechanism for noise suppression and fate stabilization. Cell 173: 1609–1621. https://doi.org/10.1016/j.cell.2018.04.005.

36. Larson DR, Zenklusen D, Wu B, Chao JA, Singer RH. 2011. Real-time observation of transcription initiation and elongation on an endogenous yeast gene. Science 332:475–478. https://doi.org/10.1126/science.1202142.

37. Takizawa T, Meaburn KJ, Misteli T. 2008. The meaning of gene positioning. Cell 135:9–13. https://doi.org/10.1016/j.cell.2008.09.026.

38. Finn EH, Pegoraro G, Brandao HB, Valton AL, Oomen ME, Dekker J, Mirny L, Misteli T. 2019. Extensive heterogeneity and intrinsic variation in spatial genome organization. Cell 176:1502–1515. https://doi.org/10.1016/j.cell.2019.01.020.

39. Price AJ, Fletcher AJ, Schaller T, Elliott T, Lee K, KewalRamani VN, Chin JW, Towers GJ, James LC. 2012. CPSF6 defines a conserved capsid interface that modulates HIV-1 replication. PLoS Pathog 8:e1002896. https://doi.org/10.1371/journal.ppat.1002896.

40. Saito A, Henning MS, Serrao E, Dubose BN, Teng S, Huang J, Li X, Saito N, Roy SP, Siddiqui MA, Ahn J, Tsuji M, Hatziioannou T, Engelman AN, Yamashita M. 2016. Capsid-CPSF6 interaction is dispensable for HIV-1 replication in primary cells but is selected during virus passage in vivo. J Virol 90:6918–6935. https://doi.org/10.1128/JVI.00019-16.

41. Kind J, Pagie L, Ortabozkoyun H, Boyle S, de Vries SS, Janssen H, Amendola M, Nolen LD, Bickmore WA, van Steensel B. 2013. Single-cell dynamics of genome-nuclear lamina interactions. Cell 153:178–192. https://doi.org/10.1016/j.cell.2013.02.028.

42. de la Vega M, Marin M, Kondo N, Miyauchi K, Kim Y, Epand RF, Epand RM, Melikyan GB. 2011. Inhibition of HIV-1 endocytosis allows lipid mixing at the plasma membrane, but not complete fusion. Retrovirology 8:99. https://doi.org/10.1186/1742-4690-8-99.

43. Delviks-Frankenberry KA, Ackerman D, Timberlake ND, Hamscher M, Nikolaitchik OA, Hu WS, Torbett BE, Pathak VK. 2019. Development of lentiviral vectors for HIV-1 gene therapy with VIF-resistant APOBEC3G. Mol Ther Nucleic Acids 18:1023–1038. https://doi.org/10.1016/j.omtn.2019.10.024.

44. He H, Xue J, Wang W, Liu L, Ye C, Cong Z, Kimata JT, Qin C, Zhou P. 2017. Efficient transduction of human and rhesus macaque primary T cells by a modified human immunodeficiency virus type 1-based lentiviral vector. Hum Gene Ther 28:271–285. https://doi.org/10.1089/hum.2016.135.

45. Jin H, Tang X, Li L, Chen Y, Zhu Y, Chong H, He Y. 2021. Generation of HIV-resistant cells with a single-domain antibody: implications for HIV-1 gene therapy. Cell Mol Immunol 18:660–674. https://doi.org/10.1038/s41423-020-00627-y.

46. Hubner W, Chen P, Del Portillo A, Liu Y, Gordon RE, Chen BK. 2007. Sequence of human immunodeficiency virus type 1 (HIV-1) Gag

localization and oligomerization monitored with live confocal imaging of a replication-competent, fluorescently tagged HIV-1. J Virol 81: 12596–12607. https://doi.org/10.1128/JVI.01088-07.

47. Muller B, Daecke J, Fackler OT, Dittmar MT, Zentgraf H, Krausslich HG. 2004. Construction and characterization of a fluorescently labeled infectious human immunodeficiency virus type 1 derivative. J Virol 78: 10803–10813. https://doi.org/10.1128/JVI.78.19.10803-10813.2004.

48. Li W, Singh PK, Sowd GA, Bedwell GJ, Jang S, Achuthan V, Oleru AV, Wong D, Fadel HJ, Lee K, KewalRamani VN, Poeschla EM, Herschhorn A, Engelman AN. 2020. CPSF6-dependent targeting of speckle-associated domains distinguishes primate from nonprimate lentiviral integration. mBio 11. https://doi.org/10.1128/mBio.02254-20.

49. van Steensel B, Belmont AS. 2017. Lamina-associated domains: links with chromosome architecture, heterochromatin, and gene repression. Cell 169:780–791. https://doi.org/10.1016/j.cell.2017.04.022.

50. Achuthan V, Perreira JM, Ahn JJ, Brass AL, Engelman AN. 2019. Capsid-CPSF6 interaction: master regulator of nuclear HIV-1 positioning and integration. J Life Sci (Westlake Village) 1:39–45. https://doi.org/10.36069/jols/20190604.

51. Schroder AR, Shinn P, Chen H, Berry C, Ecker JR, Bushman F. 2002. HIV-1 integration in the human genome favors active genes and local hotspots. Cell 110:521–529. https://doi.org/10.1016/s0092-8674(02)00864-4.

52. Wang GP, Ciuffi A, Leipzig J, Berry CC, Bushman FD. 2007. HIV integration site selection: analysis by massively parallel pyrosequencing reveals association with epigenetic modifications. Genome Res 17:1186–1194. https://doi.org/10.1101/gr.6286907.

53. Stevens TJ, Lando D, Basu S, Atkinson LP, Cao Y, Lee SF, Leeb M, Wohlfahrt KJ, Boucher W, O'Shaughnessy-Kirwan A, Cramard J, Faure AJ, Ralser M, Blanco E, Morey L, Sanso M, Palayret MGS, Lehner B, Di Croce L, Wutz A, Hendrich B, Klenerman D, Laue ED. 2017. 3D structures of individual mammalian genomes studied by single-cell Hi-C. Nature 544:59–64. https://doi.org/10.1038/nature21429.

54. Cmarko D, Verschure PJ, Martin TE, Dahmus ME, Krause S, Fu XD, van Driel R, Fakan S. 1999. Ultrastructural analysis of transcription and splicing in the cell nucleus after bromo-UTP microinjection. Mol Biol Cell 10: 211–223. https://doi.org/10.1091/mbc.10.1.211.

55. Jiang C, Lian X, Gao C, Sun X, Einkauf KB, Chevalier JM, Chen SMY, Hua S, Rhee B, Chang K, Blackmer JE, Osborn M, Peluso MJ, Hoh R, Somsouk M, Milush J, Bertagnolli LN, Sweet SE, Varriale JA, Burbelo PD, Chun TW, Laird GM, Serrao E, Engelman AN, Carrington M, Siliciano RF, Siliciano JM, Deeks SG, Walker BD, Lichterfeld M, Yu XG. 2020. Distinct viral reservoirs in individuals with spontaneous control of HIV-1. Nature 585:261–267. https://doi.org/10.1038/s41586-020-2651-8.

56. Unutmaz D, KewalRamani VN, Marmon S, Littman DR. 1999. Cytokine signals are sufficient for HIV-1 infection of resting human T lymphocytes. J Exp Med 189:1735–1746. https://doi.org/10.1084/jem.189.11.1735.

57. Yee JK, Friedmann T, Burns JC. 1994. Generation of high-titer pseudotyped retroviral vectors with very broad host range. Methods Cell Biol 43 Pt A:99–112.